The small strain stiffness of a railway ballast

Altuhafi, F.N.* & Coop, M.R.*

* University College London

Abstract

The large particle sizes of railway ballast and rock fill have meant that conventional techniques used to measure the small strain stiffness of finer geomaterials have not been adopted, with the consequence that their stiffnesses are poorly defined. In a series of tests on a UK railway ballast, simple adaptations were made to existing local strain measuring systems to account for the larger particle sizes. The study showed that the small strain stiffnesses are different in second loading compared to virgin loading, but multiple cycles had little further effect on the stiffness. The large particle size was found rarely to have any detrimental effect on the quality of the strain measurements and the two independent measurements of axial strain taken at diametrically opposite locations were generally as consistent as for finer grained soils. As for other soils, the "external" measurements of strain across the apparatus platens were of little use in determining stiffness. The presence of water did not have a significant effect on the behaviour, and this was confirmed by inter-particle loading tests on single particle contacts. Despite the use of lubricated end platens there was a significant barrelling of the sample at large shear strains so that the internal measurement of the volumetric change diverged from the external measurement at large strains. The very small volumetric **strains** that occurred during isotropic loading meant that each sample could only be used to obtain one measurement of the virgin loading stiffness.

Keywords: Ballast, Stiffness, Shearing, Triaxial.

Introduction

Railway ballast testing has received growing interest due to the importance of this material in the infrastructure of railway tracks. Laboratory based studies (Sun et al., 2019; Lackenby et al., 2007; Indraratna et al., 1998) have often provided the validation for computer simulation studies using discrete element modelling DEM (e.g. Quezada et al., 2012; Ngo et al., 2014; Ferellec et al., 2017), used then to predict the behaviour of ballast in situ. However, the available data from testing these materials is limited and does not cover all aspects of the mechanical behaviour when compared to other geomaterials with smaller particle sizes. There is a lack of information on the behaviour of ballast at small strain levels due to the large size of the particles, and neither the axial nor the volumetric strains have been well defined. The measurement of volumetric strains and hence shear strains has been particularly problematic due to very large membrane penetration (e.g. Knodel et al., 1992). Axial strains have typically been measured across the sample platens with an "external" transducer mounted outside the triaxial chamber and will be subject to the same bedding, seating, tilting and compliance errors that are seen for finer grained soils (Jardine et al., 1985). Transducers mounted locally on the sample as are common for finer grained soils (Burland & Symes, 1982; Clayton & Khatrush, 1986; Goto et al., 1991; Cuccovillo & Coop, 1997) have typically not been used.

Previous literature has shown different trials for the volumetric strain measurement of ballast samples either by the use of a direct volume gauge to measure the change in sample pore water volume for a saturated sample (e.g. Liu et al., 2008) or measuring the volume change within the triaxial chamber for a dry sample, for example by monitoring the change in level of the pressurised water surrounding the sample (Fair, 2003). Aursudkij et al. (2009) introduced the use of differential pressure to obtain the volumetric change of a dry sample through the change in volume of the pressurised fluid in a smaller chamber surrounding the sample. However, all these methods cannot overcome the inaccuracy due to membrane penetration effect for this material. A local measurement of sample circumference was advocated by Suiker et al. (2005), attaching three cable-based devices around the sample to measure the change in its circumference during the test. They then calculated the volumetric change of the dry sample depending on both the circumferential deformation and an "external" axial deformation.

The small strain stiffness is important to understand the ballast behaviour under rail track. Therefore, in this study a trial was made to measure the small strain Young's modulus and shear modulus of the material using high resolution local displacement LVDTs, scaling up techniques developed by Cuccovillo & Coop (1997) and Ackerley et al. (2016). The volumetric changes of the sample calculated from these measurements were also compared with the volumetric changes measured using an external volume gauge which is based on the volume of water entering or being expelled from a saturated sample. The aim of this work was primarily to demonstrate how local strain measurement may be made accurately on ballast or rockfill samples rather than make specific measurements for a particular rail track. The research formed part of a large research project to develop an "Avatar" DEM model of a railway ballast, the tests being used to validate the model. We therefore made no attempt to replicate the precise void ratios of a particular in-situ location or the stress levels that would typically be somewhat lower than the minimum used here. Triaxial testing at very low stresses requires other techniques to ensure the accuracy of the stresses applied (see e.g. Jovicic et al., 2006).

Within the rail track industry measurements of the ballast stiffness are generally not made directly but inferred from the in-situ measurements of the overall track stiffness, including the rail, sleeper and subgrade. This may be by shear wave velocity measurements (e.g. Zhang et al., 2020) or by back-calculation from the track displacements under a wheel load, with associated assumptions about the load transmission and deflection profile (e.g. Priest & Powrie, 2009). The ballast stiffness is then inferred from the track stiffness assuming a suitable track model and generally only the elastic stiffness is obtained. Apart from the various assumptions necessary, the problem with such approaches is that the stiffness is measured under a stress regime that is not completely known and which is highly anisotropic and variable within the ballast. It is also measured only for the void ratio achieved in-situ by the placement method. In triaxial testing the ballast fabric is unlikely to be exactly the same as that in-situ, but the stiffness can be investigated under controlled stresses, strains and void ratios, giving the degradation of stiffness from the very small strains to failure, not just the elastic value.

Tested material

The tests were carried out on a typical granite (granodiorite) ballast used in the UK railways, from the Mountsorrel quarry in Leicestershire with a mineralogy mainly consisting of quartz, potassium feldspar and plagioclase. It has a specific gravity of 2.68 (Scott and Rollinson 2015). The original particle size distribution of this material as it is used as a ballast is shown in Figure 1 with a median particle size, D_{50} of 41mm. The limited size of the sample diameter of 150mm used in this study meant that a parallel scaled grading of the same material had to be tested with a D_{50} of 21mm. This kind of parallel grading in testing rockfills and ballast is quite a common procedure (e.g. Cambio and Ge, 2007; Le Pen et al., 2013), to overcome the limitation of triaxial cell size and its compatibility with the size of particles of the tested material. Commonly a 1/3 scaling ratio is used for ballast (Aingaran et al., 2018) but a ratio of about 1/2 was preferred here, maximising the particle sizes that could reasonably tested given the sample dimensions. The literature is not clear about the effects of using a scaled ballast or rock fill compared to the original grading, with often contradictory effects for different materials (e.g. Varadarajan et al., 2003). Le Pen et al. (2013) emphasised the possible effect of differences in shape between particles of different sizes, while McDowell & Li (2016) identified that differences of particle strength could be responsible for a smaller influence of confining pressure on the peak angle of shearing resistance for the scaled ballast than for the full sized one. There may also be effects of sample size on the test data, given the relatively small ratio of sample diameter to particle size, although Hu et al. (2011) have found that these are less important in the pre-peak regime.

Apparatuses and test procedures

Triaxial apparatus

A hydraulic triaxial cell with computer-controlled pressure systems was used, which accommodates a sample with 150mm dimeter and 225mm in height. The limitation in sample height gave a ratio of height/diameter less than two but was used because of the adoption of lubricated ends. The top and lower platens were therefore made slightly larger than the sample diameter (170mm) to allow sample lateral deformation freely at both ends over the lubricated end platens (e.g. Goto and Tatsuoka, 1988; Ueng et al., 1988). Lubrication was achieved by using two layers of greased membrane at each end, making radial cuts in the rubber discs to reduce their resistance to radial strain. The membrane used in these tests both on the sample and for the lubricated ends was 1.5mm thick and they were manufactured from latex, although the sample membrane stiffness had a negligible radial restraint effect at the stress and strain levels used in these tests.

External displacement measurements were made by using a spring guided LVDT, while both cell pressure and back pressure, when applied, were monitored by pressure transducers with a maximum capacity of 10 bar. The axial displacements for shearing were applied using a constant rate of displacement system acting through the ram chamber at the lower part of the hydraulic cell (Figure 2a). A submersible load cell with a capacity of 25kN was used to measure the applied load through a half-ball system between the sample top platen and the load cell to accommodate any misalignment of the sample and load cell.

The sample was prepared in three layers within a split mould, which were subjected to vibration for 20 minutes each using an eccentric load vibrator while applying a deadweight surcharge equivalent to 5kPa on top to obtain a relatively dense sample with a void ratio of 0.7±0.01. This method was preferred over a direct compaction of the material to protect the contacts between particles from breakage that might occur under direct compaction loads. The sample was subjected to an effective stress of around 17kPa using suction through a Venturi system while removing the mould and attaching the local strain instrumentation. During the first stage of each test this suction was reduced gradually while increasing the cell pressure to minimise any significant strains in the sample. Some samples were subsequently flooded while some were tested dry. Two of the flooded samples were then saturated further under back pressure. The strains for the saturated/wet samples were monitored and found to be minimal during sample flooding and saturation stages.

Local strain measurements were made using four submersible RDP LVDTs with unguided armatures and a total stroke of ±12.5mm (model MD5/500WRA). Two were used for axial strain measurements, two for radial strain measurements. The internal axial displacement LVDTs adopted a scaled-up system similar to that of Cuccovillo & Coop (1997) but were attached to the sample using relatively large mounts (65mm x 28mm) to span several particles, based on the selected tested particle size (Figure 2a).

The radial strains were measured using the Imperial College system of Ackerley et al. (2016). This consists of an LVDT holder and a rocker arm, which translates the radial displacement of the sample into a vertical one. These are mounted on the base platen (see Figure 2b), so that the transducers move with the platen. In the original system the rocker arm rests against the sample membrane, but because of the irregular sample shape targets were made, again with a relatively large size (37mm x 62mm) that were glued to the sample membrane using a flexible silicon sealant.

Four amplifiers (RDP S7AC) were used, one for each local LVDT, and following the techniques developed by Cuccovillo & Coop (1997) immediately prior to each small strain shearing probe the potentiometers within the amplifiers were adjusted to set the output voltages of each LVDT to zero, thereby optimising their resolution. Minimum noise in the LVDT signals was ensured by shielding the cables and earthing the shields. A Datascan 7220 was used to log all the transducers, this being a datalogger that is particularly stable.

The testing procedure for the dry tests started by applying cell pressure with the pressure controller before carrying out shearing probes, typically over about 45 mins. Prior to the probes it was ensured that the rate of creep strains was less than 1% of the applied shearing rate for the probe. When multiple shearing probes were planned on the same sample, for all shearing events before the final one, care was taken to reach an axial strain that was just sufficient to show the stiffness degradation curve while minimising the loading history effect on any subsequent probe (Table 1). For Test T2 relatively large strains of 0.84-1% were applied, but these were reduced to of the order of 0.05-0.2% for most of the tests. Nevertheless, as will be discussed later, even these small strains would be too large to allow multiple probes on one triaxial sample. Some tests were also sheared to medium strains to observe the agreement of the two local strain measurements beyond the small strain region. For the wet or saturated tests, the sample was flushed with water at a cell pressure of 50kPa before increasing the cell pressure to the desired value for the test. The sample pore pressure was left open to the atmosphere in all tests except tests T9 and T9R in which the sample was saturated by increasing the cell and the back pressures with the same rate to 150 and 100kPa respectively. The isotropic compression stage followed without checking the B value as this procedure will not be meaningful for a very large membrane penetration (Knodel et al., 1992). Details of the tests are listed in Table 1. The test ID is followed by the confining pressure and condition of the test, such that T2-50Dry means that the data are from test T2 at a confining pressure of 50kPa in a dry condition.

Inter-particle apparatus

The Inter-Particle Loading Apparatus loads two particles at their contact and is described in detail by Wong & Coop (2020). It consists of 3-axis control, in the vertical and two orthogonal horizontal directions (Figure 3a). Linear actuators, load cells and displacement transducers on the three loading arms control and measure the forces and displacements applied in each direction. The actuators could control either the force or the displacement in any of the three directions by the means of the stepper motor controllers. The loads were measured by high accuracy stud load cells, which have a capacity of 1000N in the vertical direction and 500N in the horizontal direction. Very high-resolution non-contact displacement transducers were used for the displacements (Micro-Epsilon Model CSE2). These are of a capacitive type and are highly stable. A similar datalogger to that used in the triaxial apparatus, a Datascan 7250, was again employed because of its low noise and high signal stability. The apparatus stability and compliance were all checked by Wong and Coop (2020) who showed that the apparatus has very low flexibility under load while the bearing systems had very low friction.

The tested ballast particles were cut with a smooth flat surface that was attached to the top and lower platens with a high stiffness epoxy resin, using a minimal thickness of the glue to minimise compliance. Two tests were conducted using the IP apparatus to investigate the effect of water on both the normal and tangential loading stiffness (Figure 3c). The particles were prepared so that a nominal point was contacting a nominal flat. Tests details are given in Table 2. Test GB-N was carried out to investigate the effect of water on normal loading by flooding the sample during normal loading, while Test GB-CS was done by applying small cyclic tangential displacements with an amplitude of 50 microns to the contact which was normally loaded to 100N. The first four cycles were done on a dry contact then the contact was flooded and another six cycles on the flooded contact followed.

The measurement of small strain stiffness

The axial strain data for Test T2 are shown in Figure 4a. This was conducted in dry conditions and showed an excellent agreement of the two local measurements, which was typical of most tests. The figure also shows that vertical strains measured by the external LVDT are much higher than the locally measured values and cannot be used for small strain stiffness measurements any more than they can for soils of smaller particle size (Jardine et al., 1985). In Test T2, three probes at three different confining pressures were carried out at 50 kPa, 100 kPa and 150kPa respectively. The accuracy of local strain measurements at very low strains meant that a calculation of modulus of elasticity down to mean internal strains of around 0.0005% is possible. This is not as low as was achieved by Cuccovillo & Coop (1997) for finer grained soils but is adequate for most purposes.

The tangent moduli of elasticity, E, measured during the three probes in Test T2 are shown in Figure 4b. These are calculated as regressions to the stress-strain curves, taken over long enough intervals to reduce noise in the stiffnesses but not so long that the shape of the decay curve is altered, again techniques used by Cuccovillo & Coop (1997). Typical regression intervals were about 11-21 data points at the start of shearing below about 0.01% strain where there are fewer data, rising to around 51 points later in the test, the total number of data points being around 1000. The stiffnesses for the externally measured strains are clearly very much lower than those measured internally (Figure 2b). There is a clear change in behaviour from the first probe to all other consecutive probes. The E value during the first probe degraded with the progress of strain continuously, while the second and third shearing showed a persistent stable and higher value at the start of shearing followed by a distinct knee or a gross yield point before a much faster degradation. However, the volumetric strains calculated from the local displacement measurements showed only very low volumetric strains of about 0.2-0.3% for each 50kPa increase in confining pressure, so that it is likely there is only a minimal rearrangement of particles and few new particle contacts are probably produced. This low volumetric strain has been insufficient to erase the influence of the previous shearing and the probes at 100kPa and 150kPa essentially give reloading stiffnesses, in all likelihood re-loading the same contact chains through the sample established in the first shear probe. This means that unlike finer grained clays and even sands (e.g. Jovicic & Coop, 1997), multiple shearing probes on the same sample cannot be done on the same sample and a new sample is needed to investigate the behaviour at each confining pressure. In this case the probes were terminated at low axial strains (Table 1), but even had they been stopped at the minimum strain needed to define the decay curve, the strains during isotropic compression would still be insufficient to erase the influence of one probe on the next, which from experience on other soils would need to be much larger than the strains applied in the shear probes (see Jovicic & Coop, 1997).

The effect on sample void ratio of the strains applied during the probes was very small. After each shearing probe, sample relaxation was allowed overnight after unloading before carrying out the next shearing probe. Figure 5b shows the volumetric strain during the first shearing of Test T2 at 50kPa confining pressure. After the sample relaxation stage the void ratio had only changed from 0.690 to 0.691. In this probe, higher axial strains were applied during the virgin shearing stage than for other tests and for Test T6 the volumetric strains are very small indeed (Fig.5c). It is therefore not the volume change during the probes that influences the stiffness in the next probe.

The influence of one probe on subsequent probes is also consistent with the contact mechanics measured for this ballast by Altuhafi et al. (2023) and Wong & Coop (2023) where both the normal and lateral contact stiffnesses increased between first contact and the second loading but for subsequent loading cycles remained almost constant. This explanation is not incompatible with the effects of loading history on the force chains within the sample discussed above as the stiffening of the contacts that will have been deformed can explain why large volumetric strains are required between probes to disrupt those chains.

The influence of confining pressure

Figure 5a shows the degradation of tangent E with the mean internal strain during the first shearing of dry samples at various stress levels, calculated and plotted using the mean of the internal local axial strain readings. Figure 5d shows the tangent shear moduli, G for the same probes. The shear strains and hence shear stiffnesses can only be calculated from the local axial and radial strains as $\varepsilon_s = 2/3\ (\varepsilon_a - \varepsilon_r)$ since there is no externally measured volumetric strain unless a technique such a double wall cell is used (Bishop & Donald, 1961). In all these shearing probes yielding must have taken place at a very early stage at strains that were lower even than what was possible to measure using the high accuracy local strain LVDTs. In some tests, such as in the data of Test T6-100Dry in Figure 5a, some unexpected drops or jumps can be seen, which might be due to discrete effects such as individual particle movements, but generally the data are similar in nature and stability to those seen for finer grained soils. Since the shear modulus calculation in Figure 5d requires radial strains as well as axial strains to be considered, the stiffness can only be defined at slightly higher strains compared to E, typically around 0.001%.

Figure 6 shows the influence of the mean effective stress p' on the stiffness at various strain levels for all of the probes carried out. In first loading (Figure 6a) the exponent n=0.60 at the smallest resolved strains is similar to those measured for smaller grained clastic soils (sands), for example by Jovicic & Coop (1997). Membrane puncture at higher stresses restricted the stress range to a maximum of 150kPa. For most soils the contours for increasing strain levels define a series of lines, which gently converge at higher stresses, (Jovicic & Coop, 1997; Viggiani & Atkinson, 1995), but the stress range that could be applied here was too small to define this accurately, although the convergence is not very apparent. The patterns of behaviour seen in second loading are rather different (Figure 6b) and are discussed below.

Effect of water on behaviour

The effect of water on the behaviour was investigated by carrying out some tests in which the sample was flooded with water after an initial dry isotropic compression stage to 50kPa. Water flooding was done by allowing the water to enter the sample through the lower drainage port with a small pressure to ensure minimal disturbance of the sample, while the top drainage was open to atmosphere. The sample was kept open to atmosphere after flooding and during further isotropic compression and shearing in these tests, while in the two saturated Tests T9 and T9R a saturation stage was applied after flooding and a back pressure applied using 100kPa back pressure control system.

Figure 7 shows three shearing probes carried out at an effective confining pressure of 150kPa for three different sample conditions, dry, wet and saturated. In the range of data which can be measured in this study no effect of water on E can be seen. Wong & Coop (2020) had found that there is no significant effect of water on the inter-particle friction coefficient of this material when tested using the inter-particle loading apparatus. This stimulated the need to carry out some inter-particle tests on the effect of water on the particle contact at smaller displacements, particularly the stiffness during both normal loading and tangential shearing. In both Tests GB-N and GB-CS the sample was flooded half-way through the test. This is the only way to see the effect of water on inter-particle stiffness, because the differences between similar tests on different particle pairs are generally too large to see any potential effect of water. The same pair of particles could not be tested twice, once dry and once wet, because the second test would necessarily be a reloading test which has a significant effect on the stiffness (Altuhafi et al., 2023).

Figure 8a shows normal load against normal displacement during test GB-N. Flooding of sample took place at 50N normal load. No clear effect of flooding is seen on normal stiffness except the sudden temporary drop in stiffness value which coincided with the flooding process in Figure 8b, after which the stiffness value stabilizes to more or less the same value before flooding. The effect of water on the lateral stiffness of the contact is shown in Figure 9. Figure 9a shows the lateral displacement against the lateral load recorded during four lateral loading cycles in dry condition and six cycles in wet condition. The loop size reduces with cycle number and that continues after flooding, but no significant change of stiffness between dry and wet cycles can be seen. The stiffness of each cycle is calculated from the gradient of the secant passing through the two ends of each cycle (e.g. Richards et al., 2020). Figure 9b shows the change in lateral stiffness values with cycle number. The main change in stiffness occurs in the first few cycles before the flooding takes place, and there is no clear effect of flooding. The inter-particle tests therefore confirm at the particle scale what is observed at the sample size, that the presence of water has no effect on stiffness for this ballast.

Effect of cyclic shearing on small strain stiffness

Figure 10 shows the degradation curves for E obtained from four probes at 150kPa effective confining pressure, some under different conditions. Tests T3-150Dry and T7-150Dry are two virgin shearing probes on dry samples. The data shows the reasonably good repeatability of tests results between different samples. Probe T9-150Sat was carried out on virgin saturated sample with a back pressure of 100kPa, also shows strikingly similar results confirming again the repeatability and the lack of effect of water on the behaviour of this material. Probe T2-150Dry was a second shearing probe at the same pressure on a dry sample that had previously been sheared at 50kPa and 100kPa. It showed a distinctly different behaviour represented by the late yielding and the clear knee of the curve prior to the yielding point as was also seen in Figure 4. This is again seen in Figure 11 which shows four consecutive probes on dry sample T6 at an effective confining pressure of 100kPa. The difference between the second, third and the fourth probes in this test was not significant, showing that most changes in behaviour take place between the first and the second shearing probes. Figure 11b presents the volumetric strains experienced by the sample during these four probes. In general, the volumetric strains are very low and their effect on the void ratio is insignificant. It is also noted that the volumetric strains during the virgin loading event are higher than those experienced during the subsequent loading events (Figure 11b), which each give similar strains.

To investigate the effect of cyclic loading after large numbers of loading cycles, 49 cycles of loading were applied after the three initial consecutive shear probes on dry sample in Test T8, followed by a final probe at Cycle 53. The period of the 49 cycles was two hours, but small strain data were not monitored during these cycles. The effective confining pressure in this test was 150kPa and the axial load was alternated between 100N and 2100N using a control of the axial pressure via the axial hydraulic chamber rather than axial displacement to ensure that each cycle had the same magnitude in terms of axial stress. A minimum load of 100N was specified to avoid possible loss of contact between the sample and the load cell had a minimum of zero been used. Figure 12 shows the modulus of elasticity E in the first three shearing probes and also the final probe at cycle No. 53. The stiffnesses obtained after the cyclic loading stage were not very different to those obtained in the second and third shearing probes which again supports the conclusion that the main change in stiffness takes place between the first and second loading. There is perhaps a more pronounced gross yield point or knee in the data for Cycle 53. It is interesting that while the triaxial stiffnesses are essentially stable after the first loading cycle, it takes several cycles for the inter-particle shear stiffnesses to stabilise (Figure 9b).

In Figure 6b, which summarise the second loading stiffnesses for all tests and compares them with the contours defined by first loading, the stiffnesses do not change much until after 0.03% axial strain, when they drop very rapidly, the inconsistency of the data for 0.1% arising from the fact they are taken from very steep decay curves.

Volumetric strain measurements

The local strain measurements using the LVDTs showed good consistency in the range of small strains (Figure 4). To examine their consistency at moderate to high strains, loading was continued to more than 10% axial strain in Test T9 and repeated in Test T9R. Significant barrelling of the sample was however noted when higher strains were reached in spite of the lubrication of the end platens, perhaps because of the coarse nature of the ballast and hence high contact forces at local points with the platens, as could be seen from indentation of the lubrication rubber after the test. In these two saturated tests the main purpose was to compare the volumetric strains of the sample as calculated from local measurement with the volumetric strains measured by the means of an external Imperial College type volume gauge which monitored the amount of water entering or leaving the sample. Saturation of the sample was required in this test, but a B value was not calculated after the saturation stage as the effect of membrane penetration in such a material makes it meaningless. Instead, the saturation stage under 100kPa back pressure was continued until there was no further negative change in volume arising from air entering solution.

Figure 13 shows the radial and axial strains measured during Test T9R. The radial strains can only be calculated as one measurement despite using two LVDTs, unlike the local axial strains where the two LVDTs give two independent measurements. The two radial LVDT measurements cannot be regarded as being independent as both are needed to obtain one measurement of the change of sample diameter. At these larger strains than in Figure 4 there is better agreement of the external axial strain with the internal local measurements.

Figure 14 shows the volumetric strains measured using the external volume gauge compared to those values calculated from local measurements ($\varepsilon_v = \varepsilon_a + 2\varepsilon_r$). Although there is very significant membrane penetration for such a coarse material, at small strains the volumetric amount of that penetration is unlikely to change significantly under a constant effective radial stress, so it is doubtful that this is a significant factor in the divergence of the externally and internally measured volumetric strains that starts to emerge even after about 1% axial strain and barrelling is likely to be the sole cause. The agreement between the internal and external volumetric stains up to 1% is however very good. More accurate volume change measurements at larger strains would require either a more effective lubricated end platen, which seems doubtful, or measurement of the radial strain at multiple points on the sample profile.

Conclusions

Using modified designs of local strain LVDT instrumentation, measurements of tangent Young's modulus and shear modulus have been made at small strains for ballast samples down to strains of around 0.0005%. The ballast tested in this study showed distinctly different behaviour between first shearing events for a sample and consecutive shearing events, which had a later yielding point and higher values of E and G than were measured in the virgin, initial shearing event. The distinct increase of stiffness on second loading, together with only very small strains during isotropic loading meant that each sample could only be used to measure one virgin loading stiffness degradation curve. Water did not seem to be a significant factor in the stiffness behaviour of the tested ballast in the triaxial tests and the contact mechanics tests revealed that this is because the presence of water does not affect the micro-scale contact stiffnesses in either normal or lateral loading. Despite the use of lubricated end platens, the samples tended to barrel at large strains, so that the volumetric strains measured by the local LVDTs were only similar to the externally made measurements at axial strains less than about 1%.

For the shear moduli, the involvement of radial strain in the calculation added an additional source of error which resulted in more scatter in the data. This is in part because the radial strain is calculated from the summation of two transducer readings while the axial strain is the mean of two values, but it could also be due to greater sensitivity of the radial strain measurement to local particle movements, which might be improved by adopting a larger sample to particle size ratio or adding additional locations of radial strain measurement.

Acknowledgments

The authors would like to thank Dr Mathias Tolomeo for his valuable help. Thanks also go to the technical staff of the UCL soil mechanics laboratory, Mr Ben Boorman and Mr Matthew Wilkinson for their technical support and fabrication of the measuring systems. This research was fully funded by EPSRC grant number EP/S026460/1, in collaboration with Professor G.R. McDowell at Nottingham University and Dr A. Zervos at Southampton University.

References

Ackerley S., Standing, J. R. & Kamal, R. H. (2016) A system for measuring local radial strains in triaxial apparatus. Géotechnique, 66(6), 515-522.

Aingaran, S., Le Pen, L., Zervos, A. & Powrie, W. (2018) Modelling the effects of trafficking and tamping on scaled railway ballast in triaxial tests. Transportation Geotechnics, 15, 84-90.

Altuhafi, F., Baudet, B.A. & Coop, M.R. (2023) An investigation of the applicability of contact models to the normal load-deflection behaviour of artificially shaped granite. Under review for Acta Geotechnica.

Aursudkij B., McDowell G. R & Collop A. C. (2009) Cyclic loading of railway ballast under triaxial conditions and in a railway test facility. Granular Matter 11, 391–401.

Bishop, A. W. & Donald, I. B. (1961). The experimental study of partly saturated soils in the triaxial apparatus. Proc. 5th Int. Conf. Soil Mech. Found. Engng, Paris 1, 13–21.

Burland, J.B. & Symes, M. (1982) A Simple axial displacement gauge for use in the triaxial apparatus. Géotechnique, 32(1), 62-65.

Cambio, D. & Ge, L. (2007) Effects of parallel gradation on strength properties of ballast materials. Advances in Measurement and Modeling of Soil Behavior. GSP 173. https://doi.org/10.1061/40917(236)14

Clayton, C.R.I. & Khatrush, S.A (1986) A new device for measuring local axial strains on specimens. Géotechnique, 36(4), 593-597.

Cuccovillo, T. & Coop, M.R. (1997) The Measurement of Local Axial Strains in Triaxial Tests Using LVDTs. Géotechnique, 47(1), 167-171.

Fair P. (2003) The geotechnical behaviour of ballast materials for railway track maintenance. Ph.D. dissertation, University of Sheffield.

Ferellec, J. F., Perales, R., Nhu, V. H., Wone, M. & Saussine, G. (2017) Analysis of compaction of railway ballast by different maintenance methods using DEM. In Powders and Grains 2017: Proc. 8th Int. Conf. Micromechs Granular Materials, EPJ web of conferences, Vol. 140, paper No. 15032, https://doi.org/10.1051/epjconf/201714015032. Les Ulis, France: EDP Sciences

Goto, S. & Tatsuoka, F. (1988) Effects of end conditions on triaxial compressive strength for cohesionless soil. ASTM Special Technical Publications, 692-705.

Goto, S., Tatsuoka, F., Shibuya, S., Kim, Y-S. & Sato, T., (1991) A simple gauge for local axial strai measurements in the laboratory. Soils & Foundations, 31(1), 169-180.

Hu, W., Dano, C., Hicher, P-Y., Le Touzo, J-Y., Derkx,F. & Merliot, E. (2011) Effect of Sample Size on the Behavior of Granular Materials. Geotech. Testing J., 34(3), 186-197).

Indraratna, B., Ionescu, D. & Christie, H. D. (1998) Shear behaviour of railway ballast on large-scale triaxial tests. J. Geotech. Geoenviron. Engng ASCE 124(5), 439–449.

Jardine, R.J., Fourie, A., Maswoswe, J. & Burland, J.B. (1985) Field and laboratory measurements of soil stiffness. Proc 11th Int Conf. Soil Mechs & Foundn Eng., San Francisco, 2, 511-514, Rotterdam, Balkema.

Jovicic, V. & Coop, M.R. (1997) The stiffness of coarse-grained soils at small strains. Géotechnique, 47(3), 545-561.

Jovicic, V., Coop, M.R. & Simpson, B. (2006) Interpretation and modelling of deformation characteristics of a stiff North Sea clay. Can. Geotech. J. 43(4), 341-354.

Knodel, P., Bohác J.R & Feda, J. (1992) Membrane penetration in triaxial tests. Geotechnical Testing Journal, I5, 288-294.

Le Pen, L.M., Powrie, W. & Zervos, A. (2013) Dependence of shape on particle size for a crushed rock railway ballast, Granular Matter, 15(6), 849-61.

Liu, H., Deng A. & Yang, S. (2008) Shear behavior of coarse aggregates for dam construction under varied stress paths, Water Science & Engineering, 1(1), 63-77.

Lackenby, J., Indraratna, B., McDowell, G. & Christie, D. (2007) Effect of confining pressure on ballast degradation and deformation under cyclic triaxial loading. Géotechnique 57(6), 527–536, https://doi.org/10.1680/geot.2007.57.6.527.

McDowell, G.R. & Li, H. (2016) Discrete element modelling of scaled railway ballast under triaxial conditions. Granular Matter, 18:66.

Ngo, N. T., Indraratna, B. & Rujikiatkamjorn, C. (2014) DEM simulation of the behaviour of geogrid stabilised ballast fouled with coal. Comput. Geotech. 55, 224–231.

Quezada, J. C., Breul, P., Saussine, G. & Radjai, F. (2012). Stability, deformation, and variability of granular fills composed of polyhedral particles. Phys. Rev. E 86, (3), 031308.

Priest, J.A. & Powrie, W. (2009) Determination of dynamic track modulus from measurement of track velocity during train passage. J. Geotech. Geoenviron. Eng., 135, 1732-1740.

Richards, I., Byrne, B. W. & Houlsby, G. T. (2020) Monopile rotation under complex cyclic lateral loading in sand. Géotechnique, 7 (10), 916-30.

Scott, P.W. & Rollinson, G.K. (2015) Crushed rock aggregates: their mineralogy and textures using automated scanning electron microscopy. In E. Hunger and T.J. Brown (eds.), Proc. 18th Extractive Industry Geology Conf., 2014. EIG Conferences, 49-68.

Suiker, A. S. J, Selig, E.T., Frenkel, R. (2005) Static and Cyclic Triaxial Testing of Ballast and Subballast. J. of Geotech. and Geoenvir. Engineering, 131(6), 771-782.

Sun, Q. D., Indraratna, B. & Ngo, N. T. (2019). Effect of increase in load and frequency on the resilience of railway ballast. Géotechnique 69(9), 833-840.

Ueng, T. S, Tzou, Y.M. & Lee, C.J. (1988) The effect of end restraint on volume change and particle breakage of sands in triaxial tests, J. ASTM Special Technical Publications, 679-91.

Varadarajan, A., Sharma, K.G., Venkatachalam, K. & Gupta, A.K. (2003) Testing and Modeling Two Rockfill Materials. J. Geotech. & Geoenvironmental Eng., 129(3), 206-218.

Viggiani, G. & Atkinson, J.H. (1995) Stiffness of fine-grained soil at very small strains. Géotechnique, 45(2), 249-265.

Wong, C.P.Y & Coop, M.R (2020) Development of inter-particle friction in a railway ballast Géotechnique Letters, 10(4), 535-541.

Wong, C.P.Y. & Coop, M.R (2023) The Contact Mechanics of a UK Railway Ballast. Under review for Géotechnique.

Zhang, X., Thompson, D., Jeong, H., Toward, M., Herron, D., Jones, C. & Vincent, N. (2020) Measurements of the high frequency dynamic stiffness of railway ballast and subgrade. J. Sound & Vibration, 468, 3 March, 115081.

Notation

D_{50}	Particle size diameter corresponding to 50% passing of the total grading.
E	Modulus of elasticity of the material.
G	Shear stiffness modulus.
N	Normal inter-particle force.
p'	Mean effective stress.
q	Deviator stress.

T Tangential inter-particle force

ε_a Axial strain

ε_r Radial strain.

ε_s Shear strain.

ε_v Volumetric strain.

Table 1. The triaxial tests

Test ID	Condition	Effective stress for the shear probes (kPa)	Axial strains reached	Notes
T2	Dry	50, 100, 150	0.84%, 0.99%, 1.97%	
T3	Dry /wet	150_Dry, 150_Wet	1.2%, 1.6%	1st probe on dry sample then sample flooded and 2nd probe after stabilising stage
T4	Wet	150	1.8%	Isotropic compression to 150kPa dry then flooded and left to stabilise before probe
T5	Dry	100	1.27%	
T6	Dry	100	0.19%, 0.14%, 0.14%, 0.12%	Four probes at 100kPa
T7	Dry	150	0.17%	
T8	Dry	150	0.1%, 0.05%, 0.05%	3 probes, to reach a maximum load of 2088N then cyclic loading for 49 cycles, then probe 53
T9, T9R	Saturated/ back pressure 100kPa	150	Taken to higher axial strains	Tests for volumetric strain comparison

Table 2. The tests using the Inter-Particle Loading Apparatus

Test ID	Normal Load (N)	Shear displacement amplitude (μm)	Details
GB-N	100	----	Contact was vertically loaded in dry condition until 50N then contact was flooded with water and loading was continued till 100N
GB-CS	100	50	Contact was vertically loaded to 100N normal load. Cyclic loading for 4 cycles in dry condition followed by 6 cycles after flooding

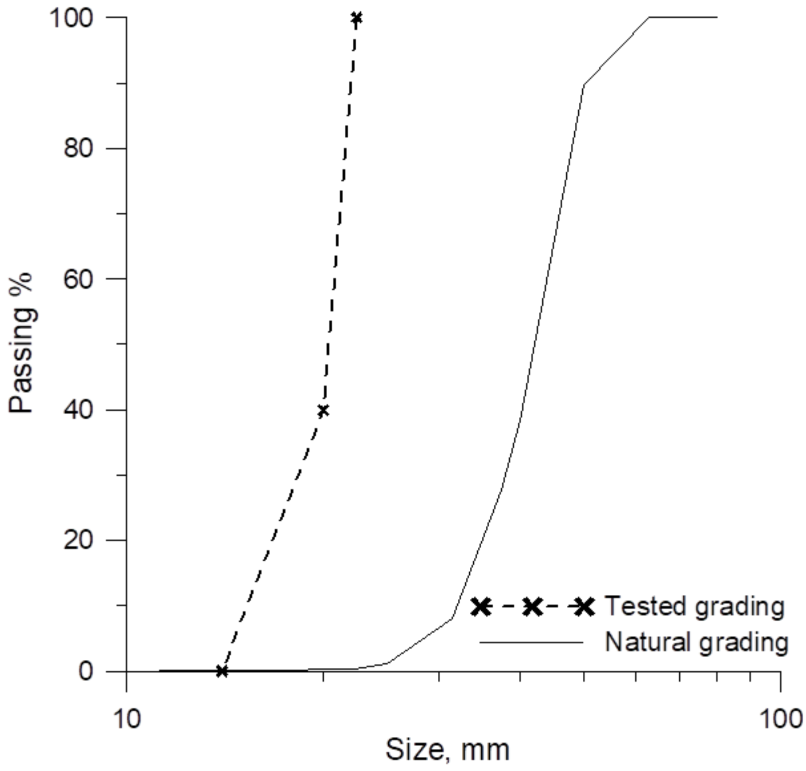

Figure 1. Gradings of the “natural” ballast and the selected scaled grading tested in this study.

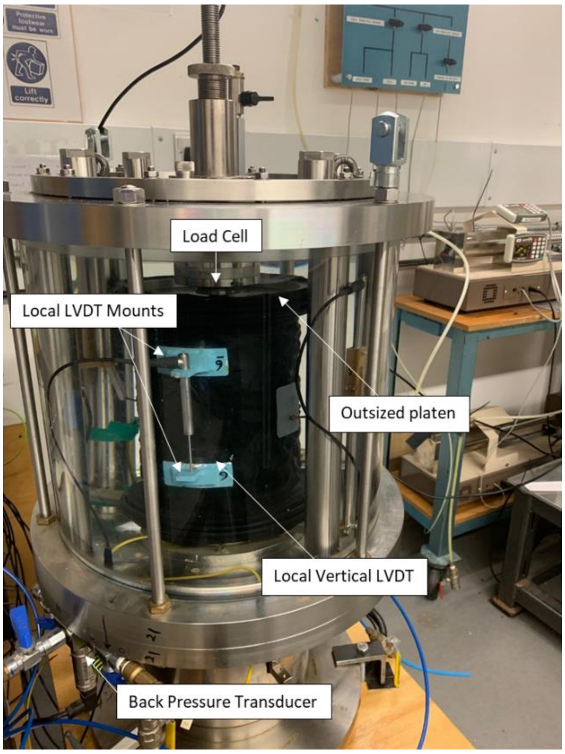

(a)

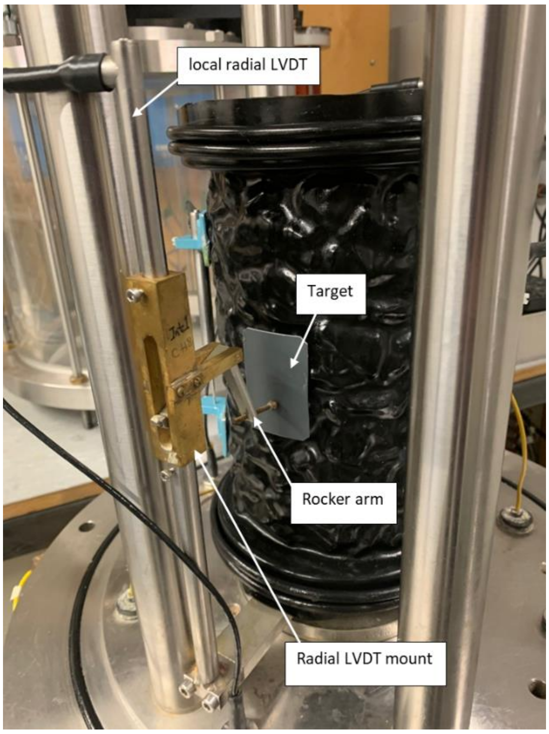

(b)

Figure 2. The triaxial apparatus, (a) local axial displacement measurement transducers, (b) local radial displacement measurement arrangement.

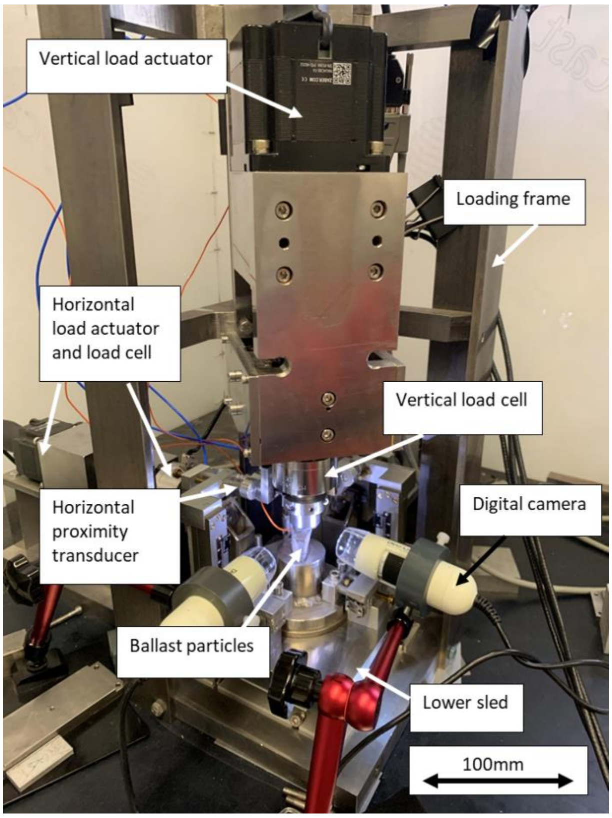
Vertical load actuator
Loading frame
Horizontal load actuator and load cell
Vertical load cell
Horizontal proximity transducer
Digital camera
Ballast particles
Lower sled
100mm

(a)

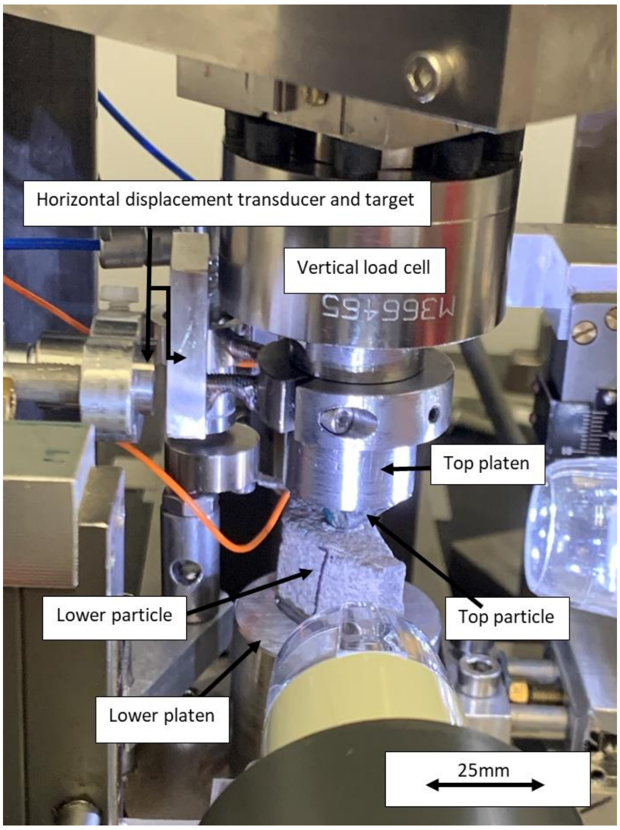
Horizontal displacement transducer and target
Vertical load cell
Top platen
Lower particle
Top particle
Lower platen
25mm

(b)

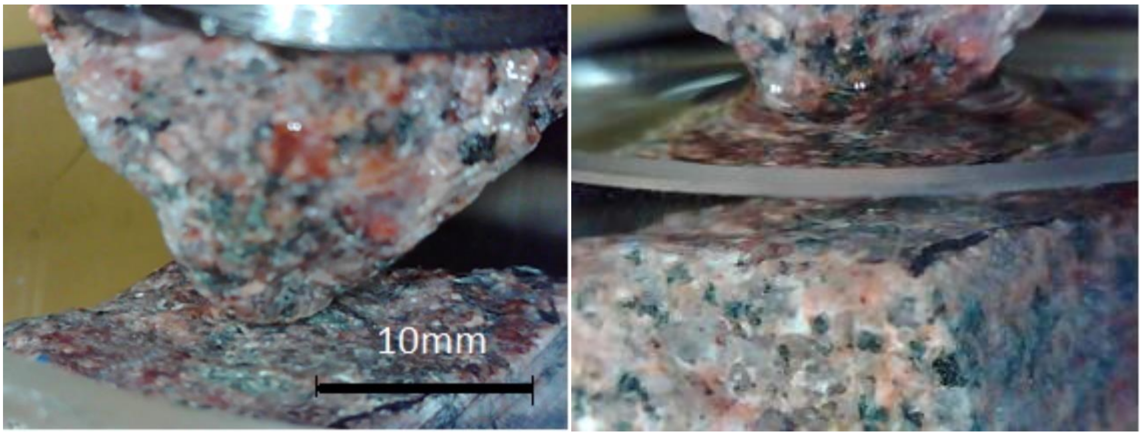

(c)

Figure 3. The Inter-Particle Loading Apparatus, (a) overall design, (b) details of the apparatus, (c) tested particles during dry and wet loading stages.

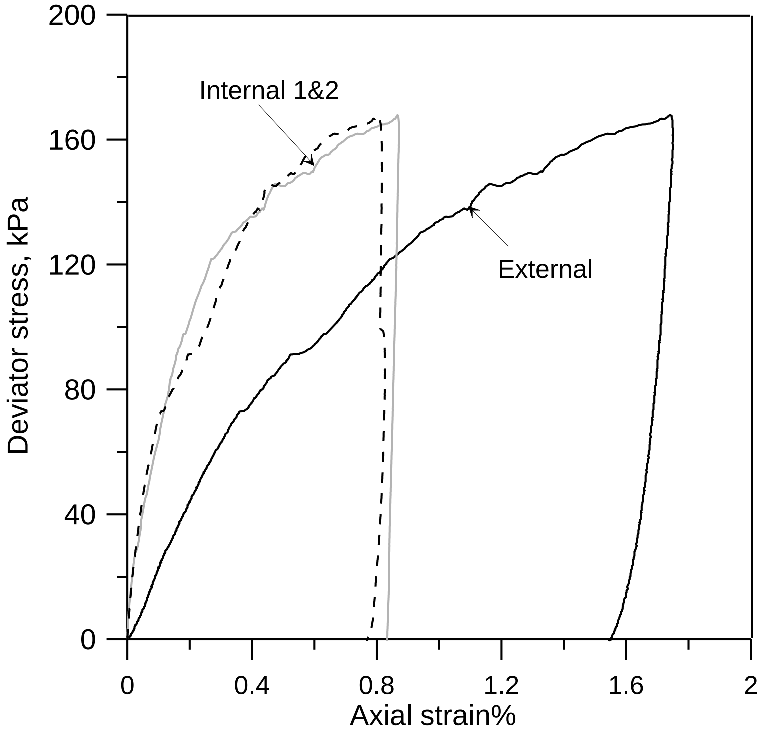

(a)

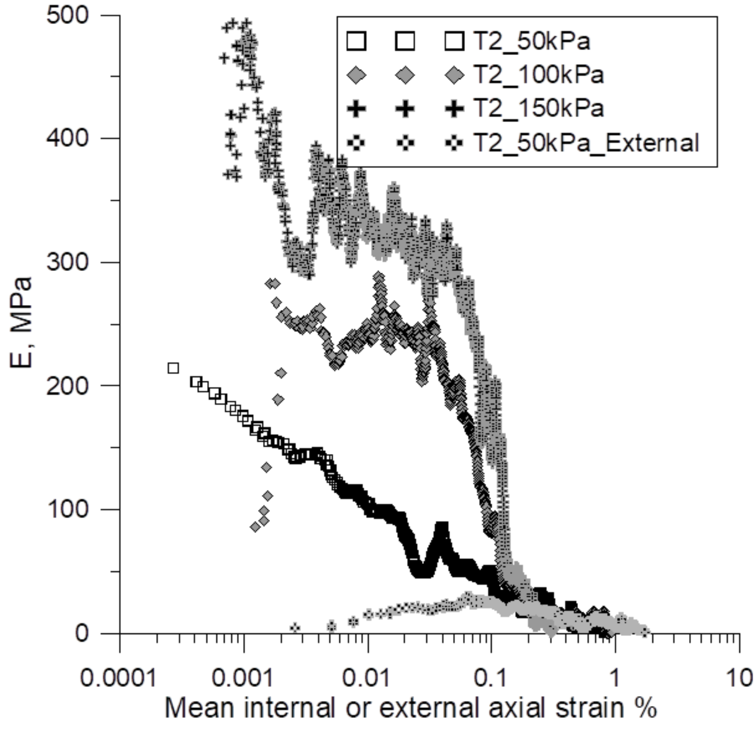

(b)

Figure 4. Data from dry Test T2 (a) comparison between external and internal LVDT readings at 50kPa, (b) tangent Young’s moduli for probes at 50, 100 and 150kPa.

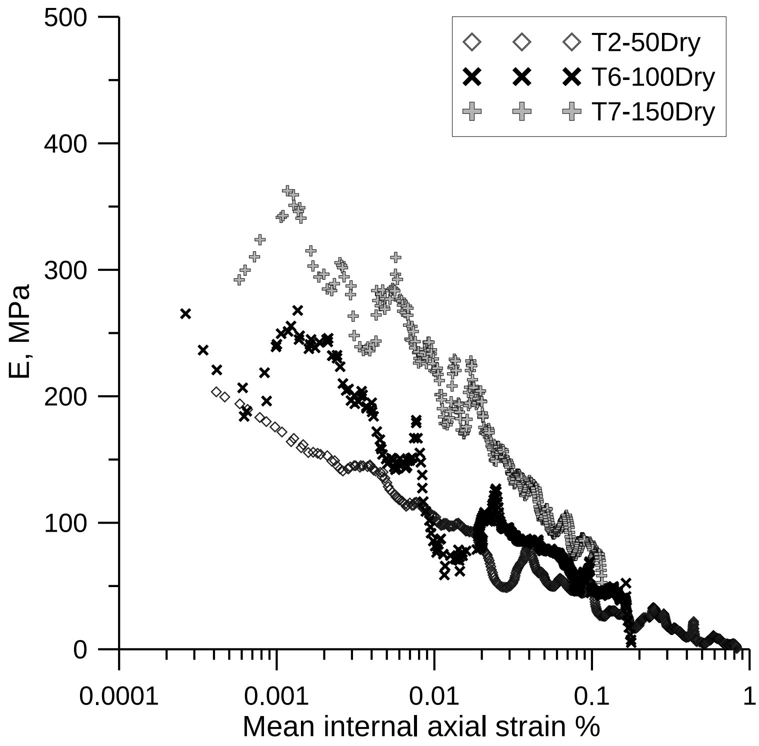
500
400
300
200
100
0
E, MPa
T2-50Dry
T6-100Dry
T7-150Dry
0.0001
0.001
0.01
0.1
1
Mean internal axial strain %

(a)

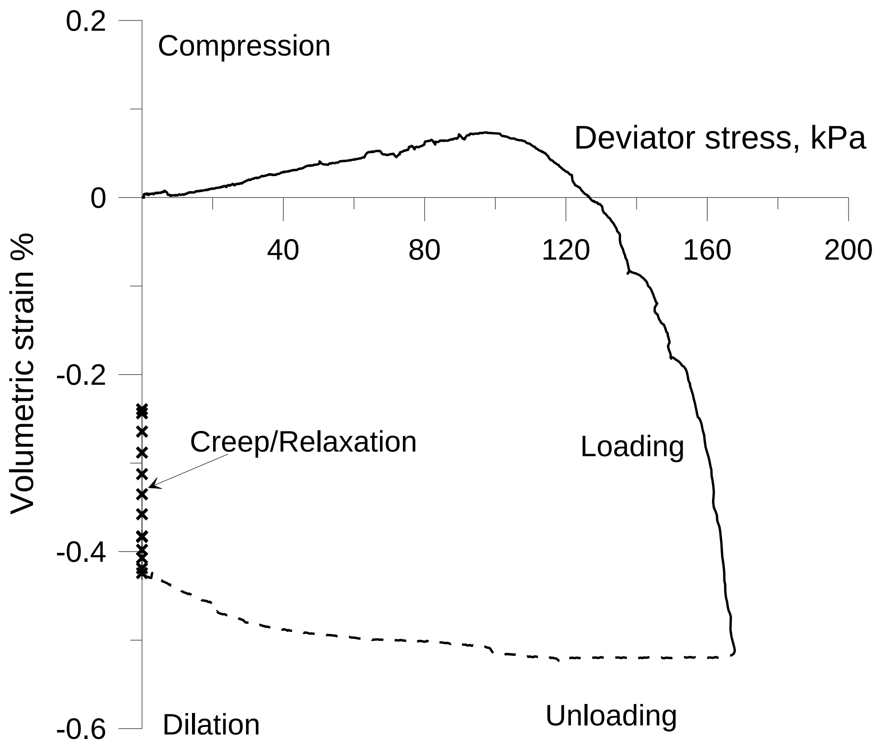
0.2
Compression
Deviator stress, kPa
0
40
80
120
160
200
Volumetric strain %
-0.2
Creep/Relaxation
Loading
-0.4
-0.6
Dilation
Unloading

(b)

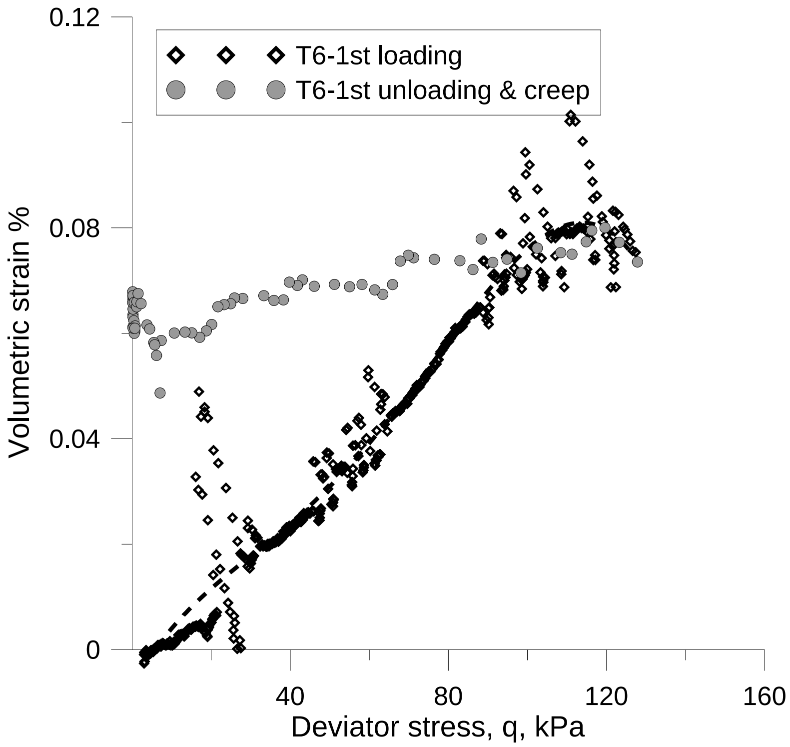

(c)

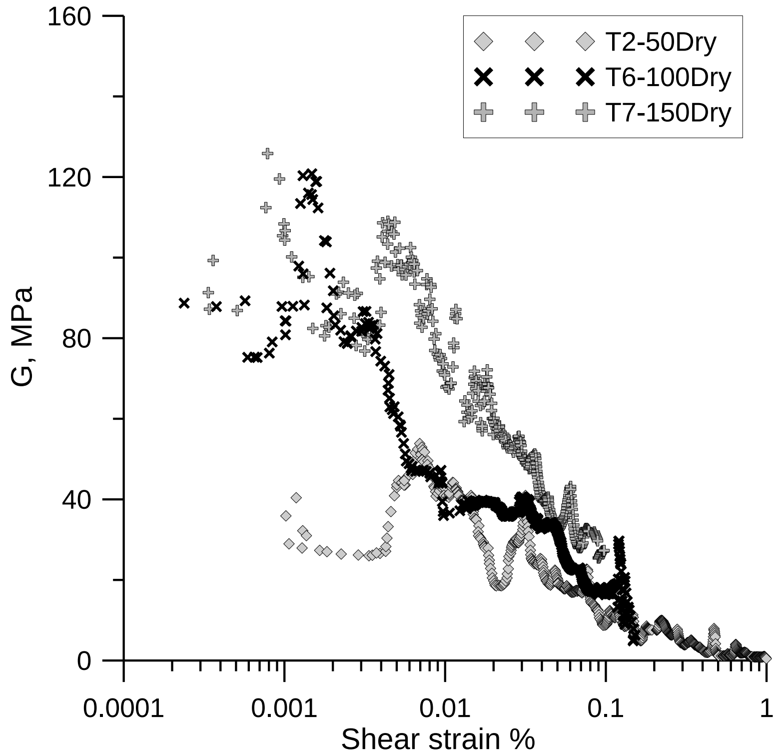

(d)

Figure 5. Data from virgin loading stage of Tests: T2, T6 and T7 during shearing at three different confining pressures (50, 100 and 150 kPa) in dry conditions (a) Degradation of tangent Young's moduli (b) volumetric change during loading cycle of virgin loading of T2 at 50kPa confining pressure (c) volumetric change during loading cycle of virgin loading of T6 at 100kPa confining pressure (d) tangent shear moduli.

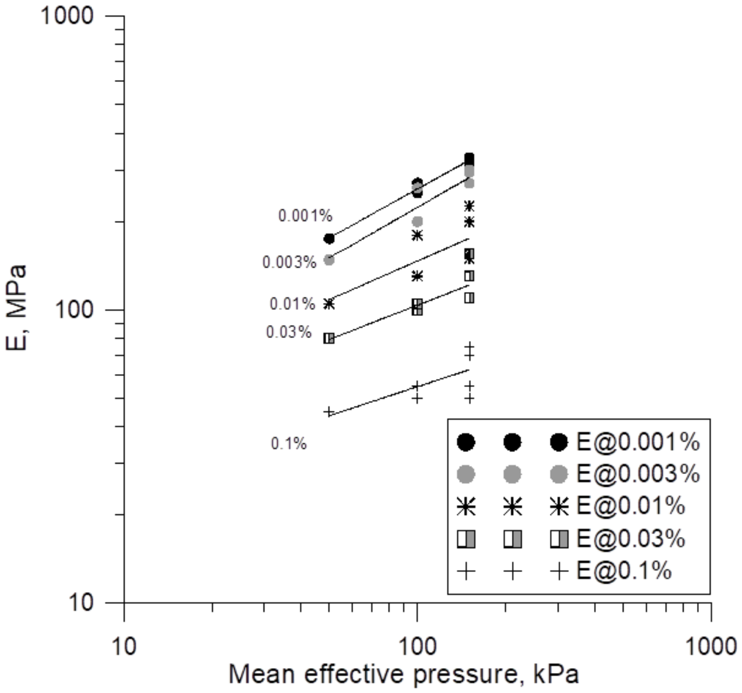

(a)

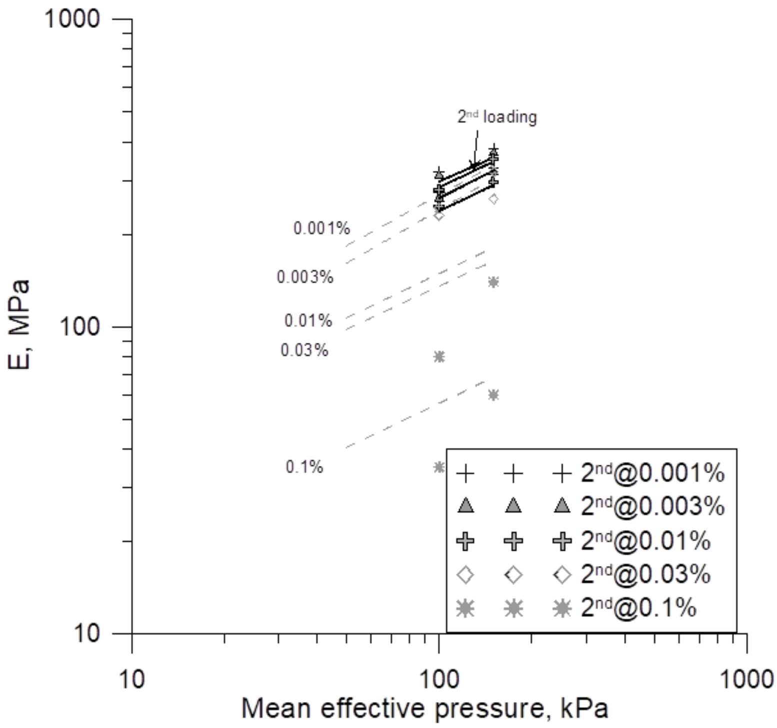

(b)

Figure 6. The influence of effective confining pressure on Young's modulus (a) first loading tests (b) reloading tests with trends from 1st loading shown.

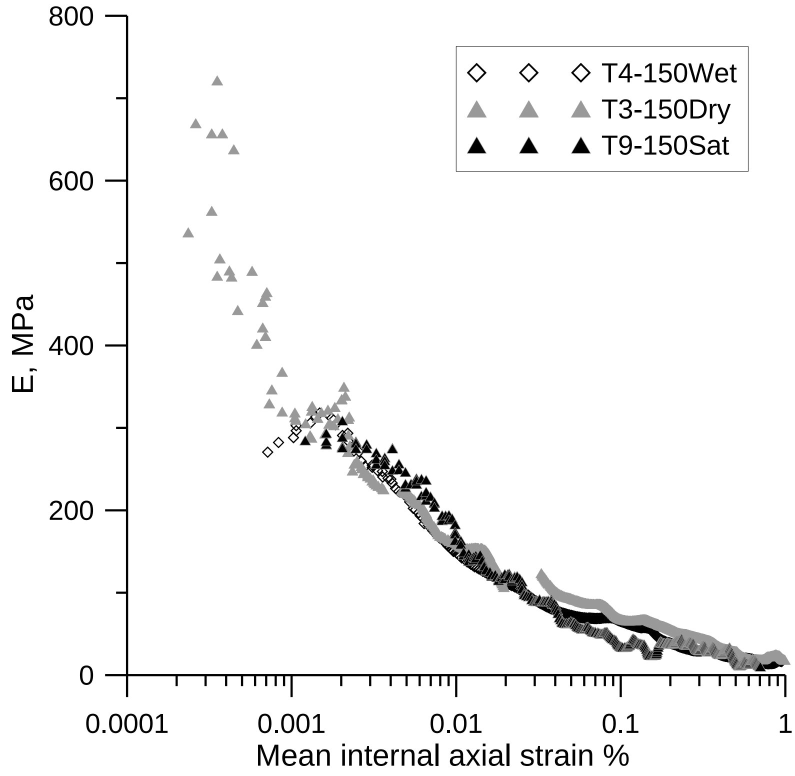

Figure 7. The effect of water on the shearing probe data at 150kPa. Test T4-150Wet on a flooded sample (zero back pressure), T3-150Dry in dry condition and T9-150Sat on saturated sample with 100kPa back pressure.

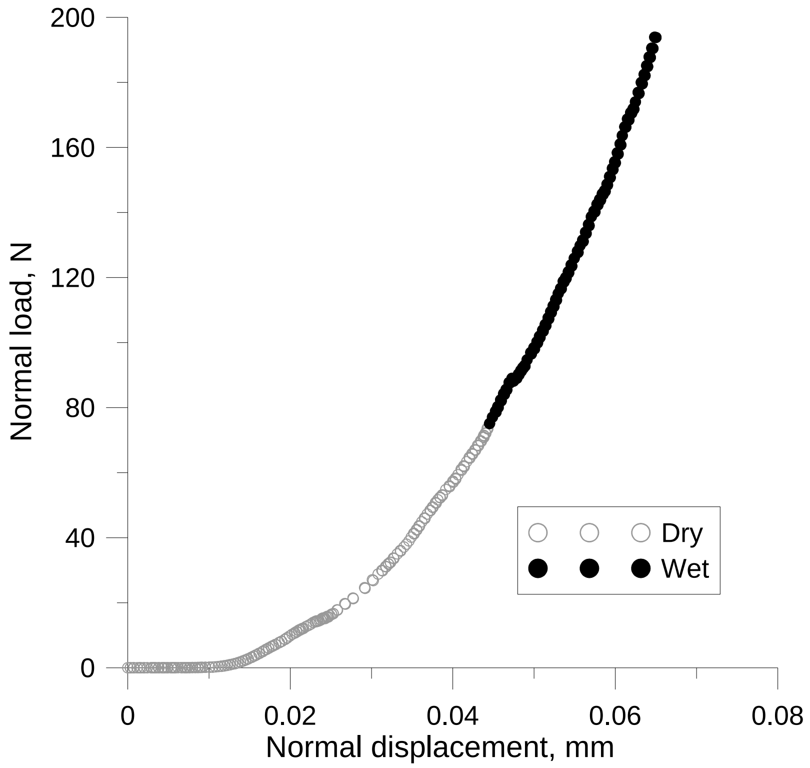

(a)

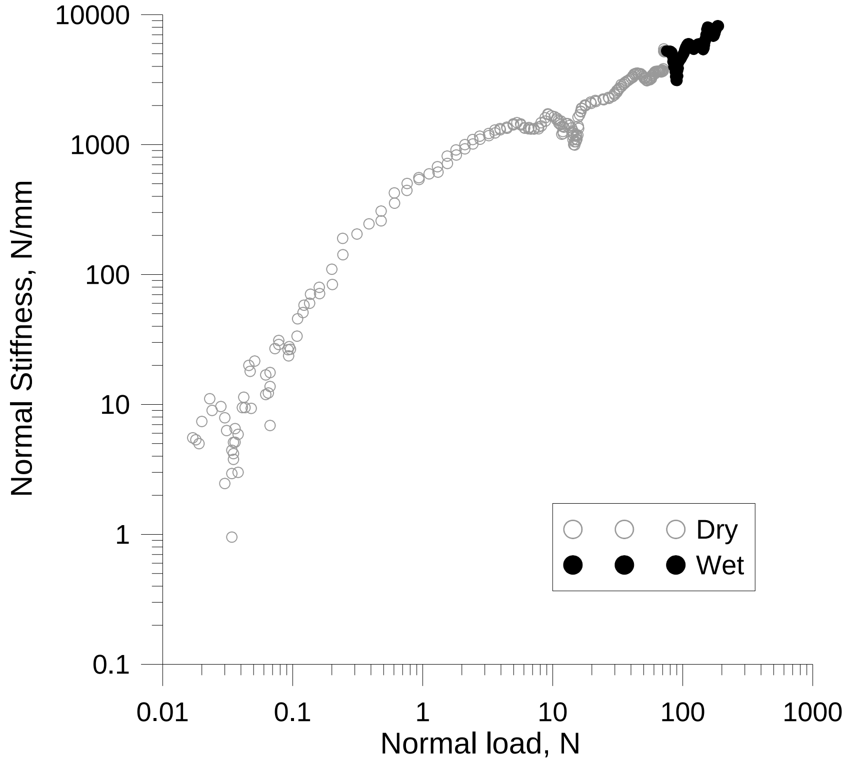

(b)

Figure 8. Effect of water during normal loading at a particle contact (a) force-displacement curve (b) force stiffness relationship.

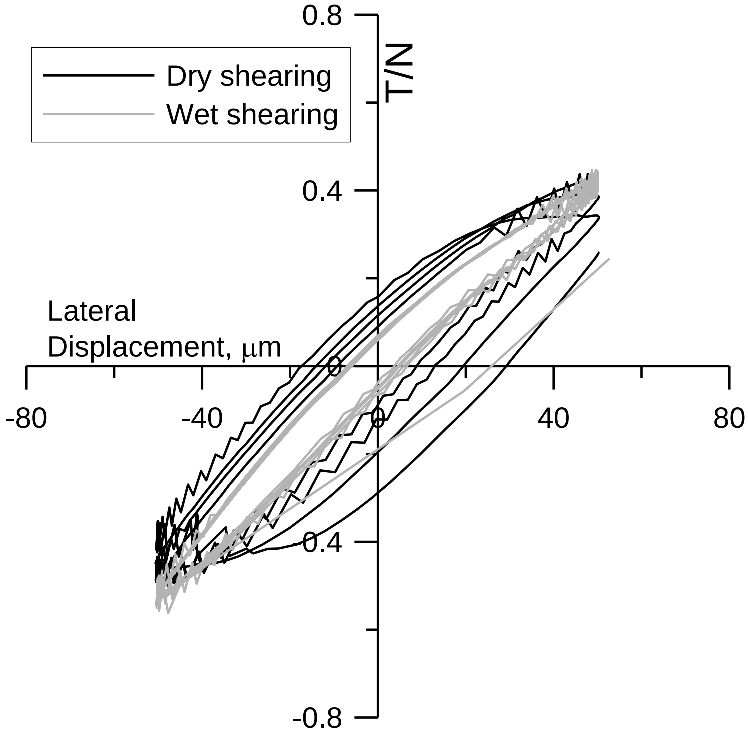

(a)

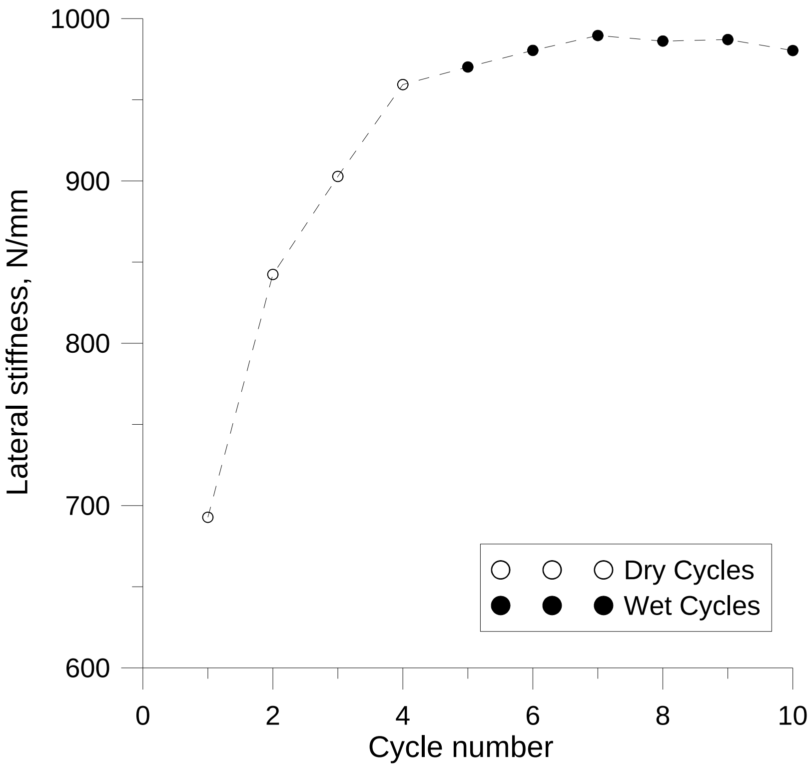

(b)

Figure 9. Pre-sliding failure lateral loading cycles under both dry and wet conditions at a particle contact (a) shear to normal force ratio (T/N) change with lateral displacement (b) lateral stiffness change with cycle number.

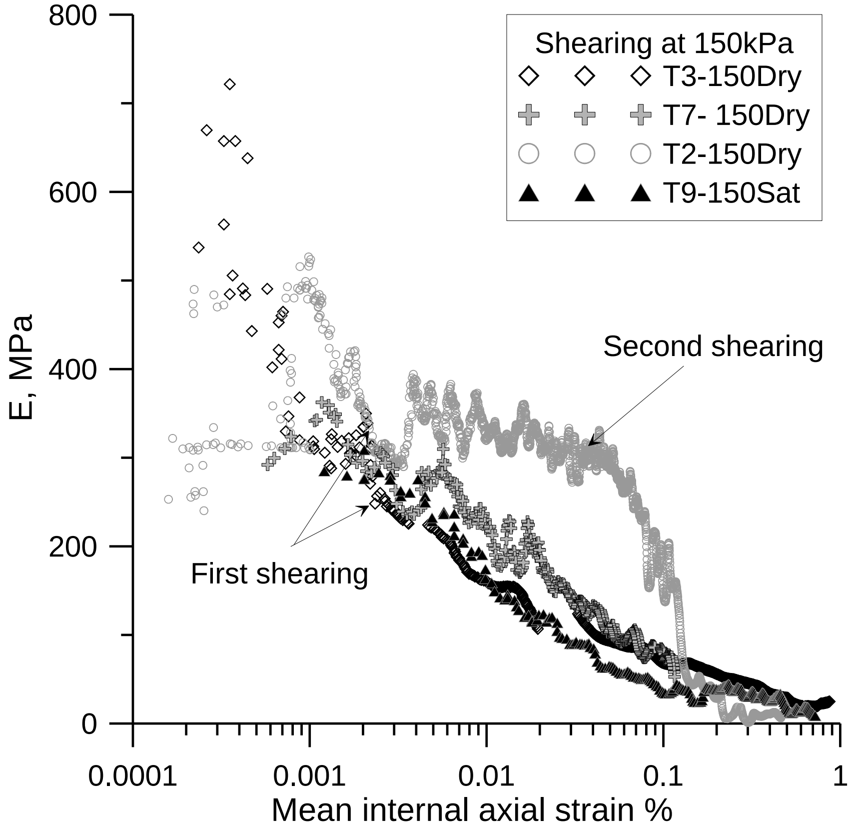

Figure 10. Comparison between initial tangent Young's moduli and second shearing stiffnesses during shearing probes at 150kPa confining pressure.

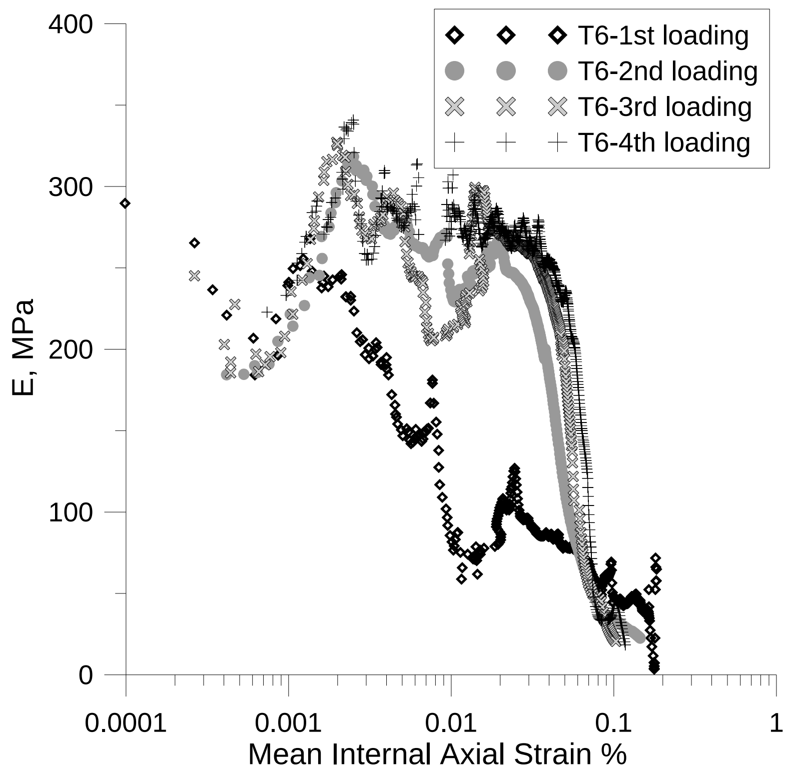

T6-1st loading
T6-2nd loading
T6-3rd loading
T6-4th loading
400
300
200
100
0
E, MPa
0.0001
0.001
0.01
0.1
1
Mean Internal Axial Strain %

(a)

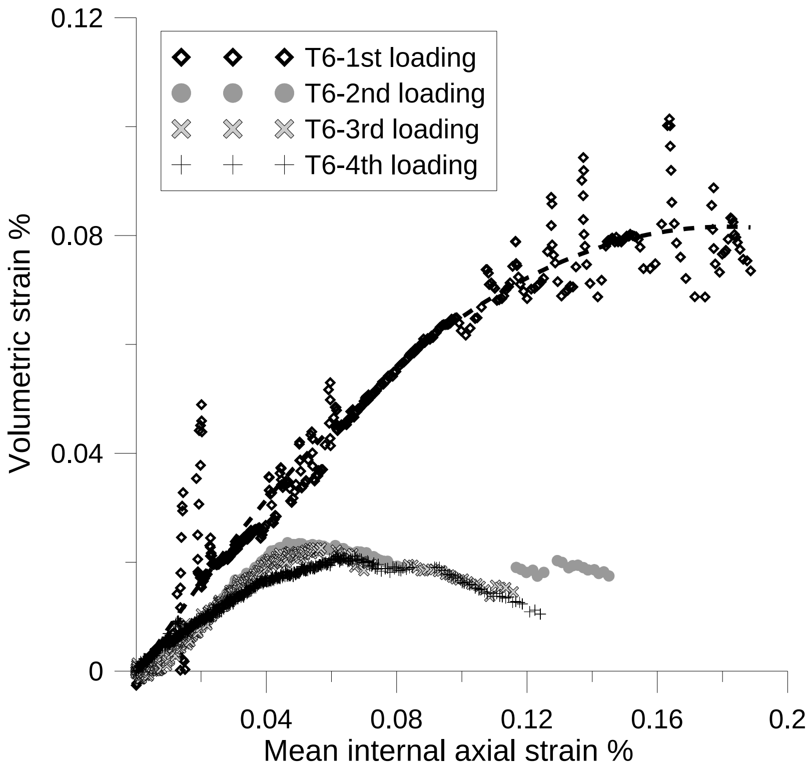

T6-1st loading
T6-2nd loading
T6-3rd loading
T6-4th loading
0.12
0.08
0.04
0
Volumetric strain %
0.04
0.08
0.12
0.16
0.2
Mean internal axial strain %

(b)

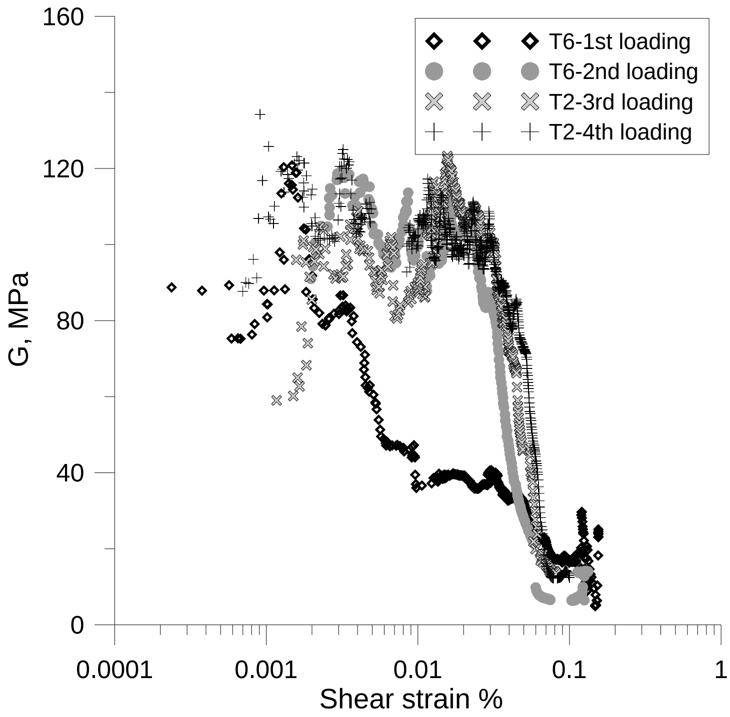

(c)

Figure 11. Effect of repeated loading for dry Test T6 at 100kPa (a) Young's moduli (b) volumetric strains (c) shear moduli.

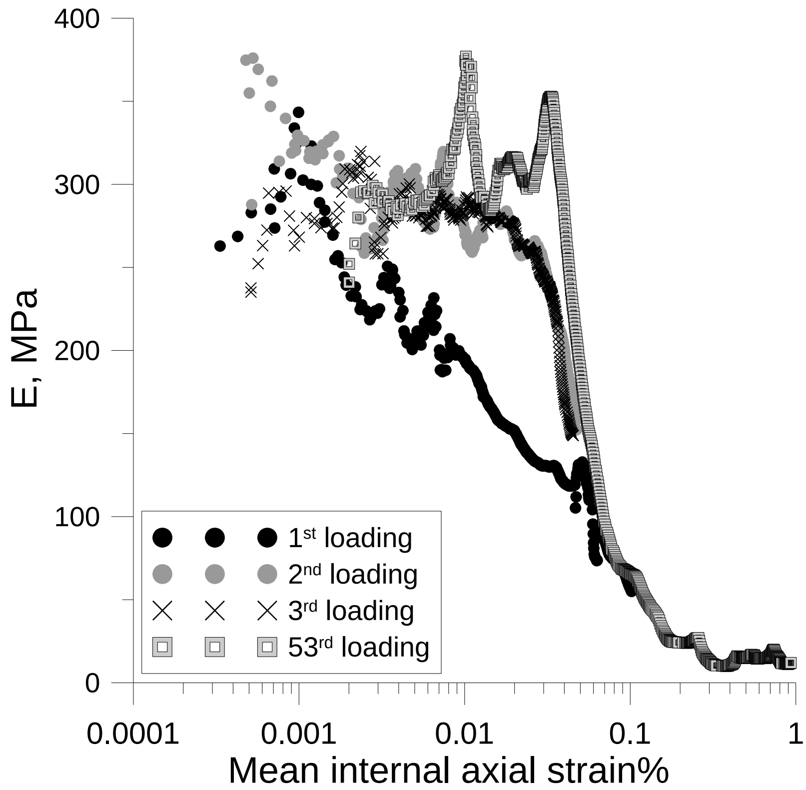

Figure 12. Tangent Young's moduli changes during the first, second and third shearing and after cyclic loading (53rd loading) in Test T8.

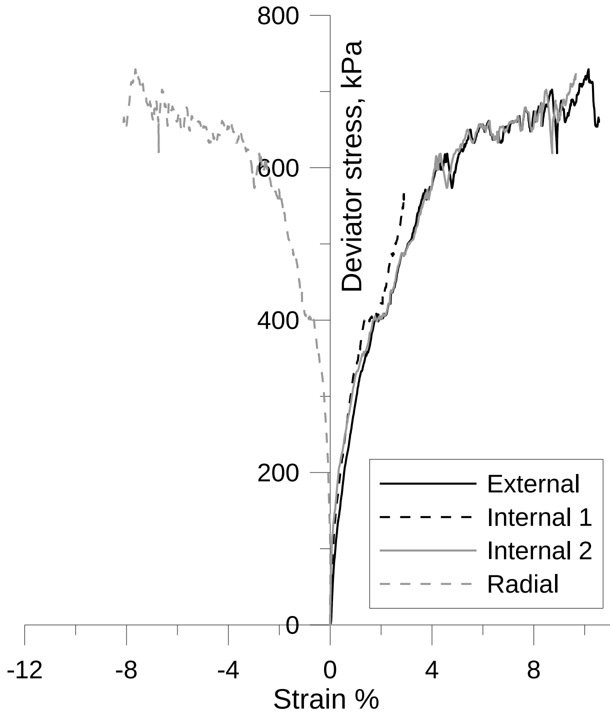

Figure 13. External and internal axial strain and internal radial strain changes during Test T9R.

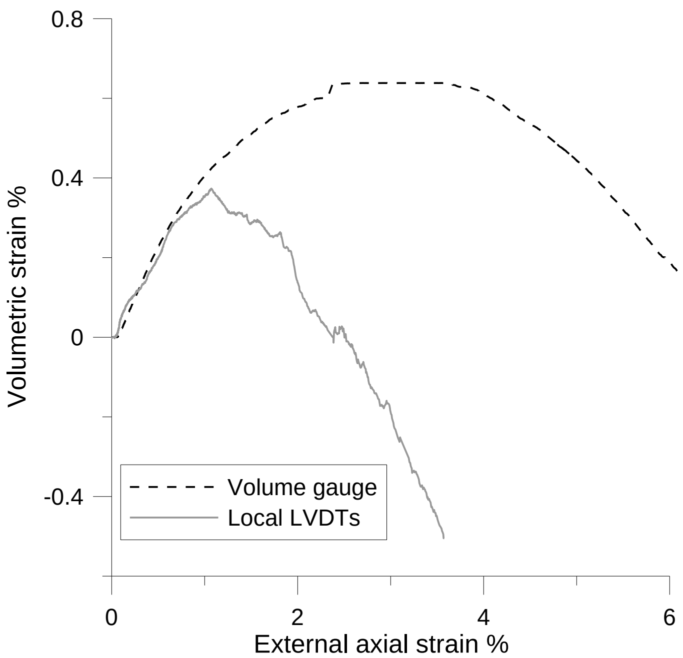

Figure 14. Volumetric strain measurement comparison for Test T9R.